Elucidating the impacts of aerosol radiative effects on surface O3 and PM2.5 for air pollution mitigation strategy in Delhi, India

Lakhima Chutia[1], Jun Wang[2], Huanxin Zhang[3], Lorena Castro Garcia[4], and Nathan Janechek[3]

[1]University of Iowa
[2]the University of Iowa
[3]403 IATL
[4]The University of Iowa

December 20, 2022

Abstract

Atmospheric aerosol radiative effects regulate surface air pollution (O3 and PM2.5) via both the aerosol–photolysis effect (APE) and the aerosol–radiation feedback (ARF) on meteorology. Here, we elucidate the roles of APE and ARF on surface O3 and PM2.5 in the heavily polluted megacity, Delhi, India by using a regional model (WRF-Chem) with constraints from available and limited observation. While APE reduces surface O3 (by 6%) and PM2.5 concentrations (by 2.4% via impeding the secondary aerosol formations), ARF contributes to a 17.5% and 2.5% increase in surface PM2.5 and O3, respectively. The synergistic APE and ARF impact contributed to ~1 % of the total concentrations of O3 and PM2.5. Hence, the reduction of PM2.5 may lead to O3 escalation due to weakened APE. Sensitivity experiments indicate the need and effectiveness of reducing VOC emission for the co-benefits of mitigating both O3 and PM2.5 concentrations in Delhi.

Hosted file

`952095_0_art_file_10546153_rn456b.docx` available at https://authorea.com/users/567859/articles/613986-elucidating-the-impacts-of-aerosol-radiative-effects-on-surface-o3-and-pm2-5-for-air-pollution-mitigation-strategy-in-delhi-india

Hosted file

`952095_0_supp_10546154_rn456b.docx` available at https://authorea.com/users/567859/articles/613986-elucidating-the-impacts-of-aerosol-radiative-effects-on-surface-o3-and-pm2-5-for-air-pollution-mitigation-strategy-in-delhi-india

1

Elucidating the impacts of aerosol radiative effects on surface O$_3$ and PM$_{2.5}$ for air pollution mitigation strategy in Delhi, India

Lakhima Chutia[1, 2]*, Jun Wang[1, 2]*, Huanxin Zhang[1, 2], Lorena Castro Garcia[1, 2], Nathan Janechek[2]

[1]Department of Chemical and Biochemical Engineering, College of Engineering, University of Iowa, IA, USA

[2]Iowa Technology Institute and Global and Regional Environmental Research, College of Engineering, University of Iowa, IA, USA

*Corresponding author: Jun Wang, jun-wang-1@uiowa.edu;

Lakhima Chutia, lakhima-chutia@uiowa.edu

Key points:

- The aerosol–photolysis effect contributes to a reduction in surface O$_3$ and PM$_{2.5}$ concentration in Delhi during post-monsoon.
- The aerosol–radiation feedback decreases the boundary layer mixing, increases relative humidity, and aggravates surface PM$_{2.5}$ and O$_3$.
- Effective control of VOC helps in achieving both O$_3$ and PM$_{2.5}$ reductions in Delhi.

20 **Abstract**

21 Atmospheric aerosol radiative effects regulate surface air pollution (O_3 and $PM_{2.5}$) via both the

22 aerosol–photolysis effect (APE) and the aerosol–radiation feedback (ARF) on meteorology.

23 Here, we elucidate the roles of APE and ARF on surface O_3 and $PM_{2.5}$ in the heavily polluted

24 megacity, Delhi, India by using a regional model (WRF-Chem) with constraints from available

25 and limited observation. While APE reduces surface O_3 (by 6%) and $PM_{2.5}$ concentrations (by

26 2.4% via impeding the secondary aerosol formations), ARF contributes to a 17.5% and 2.5%

27 increase in surface $PM_{2.5}$ and O_3, respectively. The synergistic APE and ARF impact contributed

28 to ~1 % of the total concentrations of O_3 and $PM_{2.5}$. Hence, the reduction of $PM_{2.5}$ may lead to O_3

29 escalation due to weakened APE. Sensitivity experiments indicate the need and effectiveness of

30 reducing VOC emission for the co-benefits of mitigating both O_3 and $PM_{2.5}$ concentrations in

31 Delhi.

32 **Plain Language Summary**

33 Surface ozone (O_3) and fine particulate matter ($PM_{2.5}$) are dominant air pollutants in the megacity

34 Delhi, India. However, controlling $PM_{2.5}$ concentration by reducing emissions may have

35 unexpected consequences on O_3 because aerosols may lead to O_3 escalation by increasing

36 photolysis and at the same time reduce O_3 by increasing the solar input at the surface and hence,

37 the turbulent mixing. Here we used a regional model to quantify the separate contribution of

38 aerosol–photolysis effect (APE) and aerosol–radiation feedback (ARF) on surface $PM_{2.5}$ and O_3

39 in Delhi and further discuss the measures for reducing both $PM_{2.5}$ and O_3 levels. This study

40 elucidates the importance of APE and ARF effects in designing effective mitigation strategies for

41 both $PM_{2.5}$ and O_3 pollution. The effective control of VOC emissions is highly recommended for

42 co-controlling both O_3 and $PM_{2.5}$ levels in the megacity Delhi.

43

1 Introduction

Ground-level ozone (O_3) and fine particulate matter with aerodynamic diameter ≤ 2.5 μm or $PM_{2.5}$ are dominant air pollutants in megacities such as Delhi, India. Delhi has been experiencing severe air pollution episodes in recent years, especially during the post-monsoon (Oct. and Nov.) and winter times (Dec., Jan., and Feb.) (Bharali et al., 2019; Kulkarni et al., 2020; Kumar et al., 2020). $PM_{2.5}$ and O_3 in this region often exceed the Indian National Ambient Air Quality Standards (INAAQS) and pose a serious threat to public health (Ghude et al., 2016; Krishna et al., 2019; Sahu & Kota, 2017). $PM_{2.5}$ can lead to ~ 1 million premature deaths per year in India (Conibear et al., 2018; Ghude et al., 2016). O_3, the second major pollutant adversely impacting human health after $PM_{2.5}$ also leads to 31,000 premature mortalities per year (Ghude et al., 2016). Besides, O_3 and $PM_{2.5}$ exposure damages crops and significantly reduces wheat and rice (22–42%) yields in India (Sinha et al., 2015). Therefore, the prediction and process understanding of both $PM_{2.5}$ and O_3 are highly essential to improve the air quality and mitigate their impacts on public health and agriculture in this region.

Past studies have focused on several factors including emission, meteorology, and atmospheric chemistry governing the high concentrations of $PM_{2.5}$ and O_3 in the Indian region (Bran & Srivastava, 2017; Kulkarni et al., 2020; Ojha et al., 2020). One factor often overlooked in the literature is the impact of aerosol–radiation interaction (ARI) on both $PM_{2.5}$ and O_3 and the non-linear synergistic processes therein. The ARI influences O_3 chemistry and atmospheric oxidation capacity by modulating photolysis rates in the troposphere known as the aerosol–photolysis effect (APE) which further influences the particle formation process and air quality (Benas et al., 2013; Dickerson et al., 1997; Li et al., 2011; Liao et al., 1999; Xing et al., 2017). Modeling studies have highlighted the reduction (enhancement) in photolysis rate due to strong absorption (scattering) of aerosols (Li et al., 2005; Li et al., 2017; Liao et al., 1999, Tie et al., 2003), with subsequent effects on the O_3 formation. Several studies have analyzed the impact of APE in different parts of the world such as the urban environment in China (Xing et al., 2017; Yang et al., 2022), Mexico (Li et al., 2011), Europe (Real & Sartelet, 2011), and Texas (Flynn et al., 2010). However, such studies are still limited over the Indian region.

ARI not only entails APE but also includes aerosol–radiation feedback or ARF on meteorology that in turn affects surface O_3 and aerosol distribution. ARI can lead to a substantial decrease of solar inputs at the ground, thereby reducing surface temperature and the planetary

75 boundary layer (PBL) height. Via absorption of radiation, aerosols can heat the atmosphere,
76 increase atmospheric stability, and further enhance aerosol concentration in the PBL (Li et al.,
77 2017; Yang et al., 2020); this positive feedback via ARF is particularly significant during severe
78 pollution episodes (Bharali et al., 2019; Liu et al., 2018; Wang et al., 2020; Zhao et al., 2019).

79 To study the air pollution mitigation strategy in Delhi, India, here we employ a regional
80 chemistry transport model (WRF-Chem) to elucidate the relative role of APE and ARF on
81 surface $PM_{2.5}$ and O_3 in the National Capital Region (NCR) of India. WRF-Chem has been
82 widely used for the simulation of $PM_{2.5}$ and O_3 across the Indian region (Bran & Srivastava,
83 2017; Jat et al., 2021; Mogno et al., 2021; Ojha et al., 2020; Sharma et al., 2017; Upadhyay et al.,
84 2018). But only a few studies have focused on the impacts of ARF (Kumar et al., 2020; Bharali
85 et al., 2019) with no study analyzing the pure and synergistic effect of APE and ARF. Kumar et
86 al. (2020) showed that the inclusion of ARF in WRF-Chem can lead to a significant
87 improvement in the $PM_{2.5}$ forecast by reducing the mean bias up to 25% in NCR Delhi.
88 Mukherjee et al. (2020) found a 30% reduction in surface O_3 concentration due to the APE
89 associated with black carbon over South Asia. Hence, while reducing black carbon may lead to a
90 decrease in $PM_{2.5}$, it may lead to an increase in surface O_3 concentration. The overall net effects
91 of APE and ARF on both O_3 and $PM_{2.5}$ over the Indian region remain elusive, although the air
92 pollution mitigation strategy requires scientific consideration of the role of both APE and ARF as
93 well as their synergistic effects.

94 Here, the pure and synergistic contributions of APE and ARF are quantitatively analyzed
95 through model sensitivity simulations with the constraint of surface observations (described in
96 section 2.2), focusing on the post-monsoon period in November 2018 over NCR Delhi. Results
97 are presented in Section 3, starting from the comparison of the model results with observations
98 (Section 3.1) to the analysis of the impact of pure and synergistic APE and ARF (Section 3.2–
99 3.3). The summary and conclusions are provided in Section 4.

100 **2 Methodology**

101 **2.1 Model Description**

102 A regional model with Unified Inputs (of initial and boundary conditions) for the
103 Weather Research and Forecasting model coupled with chemistry (UI-WRF-Chem) is used to
104 simulate O_3 and $PM_{2.5}$ in Delhi in two nested domains at 12 and 4 km horizontal resolutions,

105 respectively. The outer and inner domains cover the entire northern part of the Indian
106 subcontinent and NCR Delhi, respectively (Figure S1). There are 47 vertical layers from the
107 ground to 50 hPa. The UI-WRF-Chem model utilizes MERRA-2 data to provide both
108 meteorological and chemical initial and boundary conditions. Initial conditions for soil properties
109 (soil moisture, soil temperature) are taken from the Global Land Data Assimilation System
110 (GLDAS) at a horizontal resolution of $0.25° \times 0.25°$.

111 The WRF-Chem emission preprocessing system (WEPS) designed in-house is used to
112 prepare the anthropogenic and biogenic emissions needed for UI-WRF-Chem (Sha et al., 2021;
113 Zhang et al., 2022). Anthropogenic emissions are based on Emissions Database for Global
114 Atmospheric Research - Hemispheric Transport of Air Pollution (EDGAR-HTAP) (Janssens-
115 Maenhout et al., 2015), which includes PM_{10}, $PM_{2.5}$, BC, OC, NH_3, NMVOCs, CO, NOx and
116 SO_2 at a horizontal resolution of 0.1º x 0.1º. Biomass burning emissions from the Fire Locating
117 and Modeling of Burning Emissions Inventory (FLAMBE) (Reid et al., 2009) is used to specify
118 the sources of BC, OC, and gaseous species (CO, NO_2) as a function of time (at injection height
119 of 800 m above the surface). Further details of FLAMBE and WEPS can be found elsewhere
120 (Ge, Wang, & Reid, 2013; Ge et al., 2017; Wang et al., 2013). Regional Acid Deposition Model
121 version 2 (RADM2) (Stockwell et al., 1990) coupled with the Modal Aerosol Dynamics for
122 Europe (MADE) and the Secondary Organic Aerosol Model (SORGAM) (Schell et al., 2001) are
123 used to simulate the gas-phase chemistry and aerosols. Currently, the inorganic chemistry system
124 considered in MADE is limited to sulfate, nitrate, ammonium, and water components in the
125 aerosol phase. The Fast Tropospheric UV and Visible Radiation Model (FTUV) (Li et al., 2005;
126 Tie et al., 2003) is used to evaluate aerosol effects on photolysis rates and the Goddard
127 shortwave radiative transfer module (Chou & Suarez, 1994) is employed for estimating
128 shortwave radiation. Other physics parameterization schemes (Table S1) used here are based on
129 the earlier studies using the WRF-Chem model over the Indian region (Chutia et al., 2019; Ojha
130 et al., 2020).

2.2 Simulation scenarios and analysis method

132 We utilized the factor separation approach (FSA) method (Stein & Alpert, 1993) to obtain
133 the pure contribution of APE and ARF and their synergistic contributions due to the mutual
134 interactions among APE and ARF. This method has been extensively applied in the analysis of

135   numerical simulations (Li et al., 2018; Qu et al., 2013). Based on the FSA, four simulations such

136   as BASE, NOALL, APE only, and ARF only, have been performed to quantify the pure and

137   synergistic impacts of APE and ARF on O_3 and $PM_{2.5}$ (See Table S2). In the BASE simulation,

138   the impacts of both ARF and APE are considered. In NOALL, ARF and APE are both turned off.

139   Considering that $f_{ARF+APE}$, f_{ARF}, f_{APE}, and f_0 are the simulation results including both APE

140   and ARF (i.e., BASE), ARF only, APE only, and neither APE nor ARF (i.e., NOALL),

141   respectively, one can show that the synergistic contributions between APE and ARF are as

142   follows:

143   $$f'_{ARF+APE} = f_{ARF+APE} - f_{APE} - f_{ARF} + f_0 \qquad\qquad (i)$$

144   Each simulation is performed from 22 October to 30 November 2018 with the first 10 days as the

145   model spin up.

2.3 Observational Data

147   Ground-based measurements of $PM_{2.5}$, O_3, and meteorological parameters (temperature and

148   relative humidity) at different stations over NCR Delhi (Figure S1b) are obtained from the

149   Central Pollution Control Board (CPCB), India. The instruments are periodically calibrated, and

150   measurements are regularly checked and controlled with quality assurance by the CPCB

151   (cpcb.nic.in/quality-assurance-quality-control/). Additional data assurance is considered by

152   removing very high (> 1500 mg m^{-3}) and low (< 10 mg m^{-3}) $PM_{2.5}$ values following Kumar et al

153   (2020).

3   Results

3.1 Model evaluation

156   The BASE and NOALL simulations are first used for the evaluation of overall impact of

157   ARI on the model results. The diurnal pattern and magnitude of 2 m air temperature (T2) and

158   relative humidity (RH) are captured well by the UI-WRF-Chem in both simulations, with a

159   relatively smaller bias in the BASE case (Figure 1a–b and Table S3). The normalized mean bias

160   (NMB) between the observation and model is reduced from –11% in NOALL to –5% in the

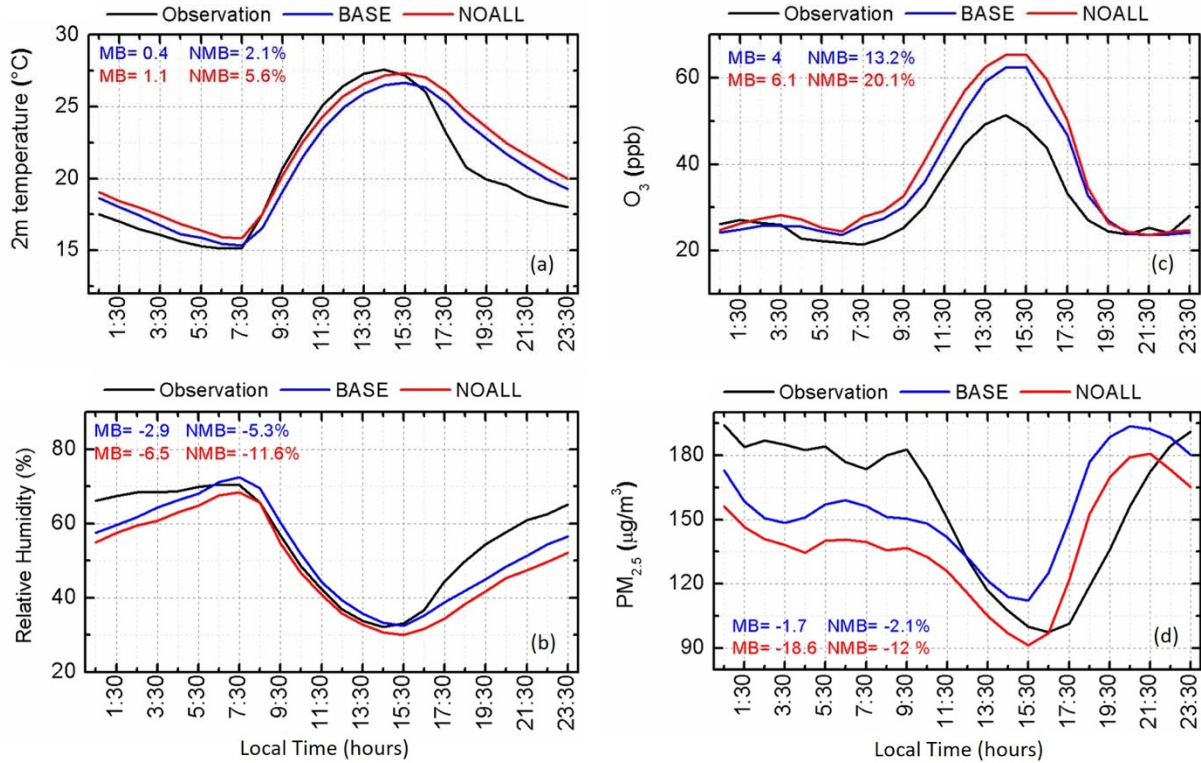161   BASE for RH and 5% to 2% for T2.

Figure 1. Diurnal variation of observed (black) and simulated variables (blue for BASE and red for NOALL experiments). **(a)** 2m temperature (° C), **(b)** relative humidity (%), **(c)** O_3 (ppb), and **(d)** $PM_{2.5}$ ($\mu g\ m^{-3}$) in megacity Delhi during November 2018.
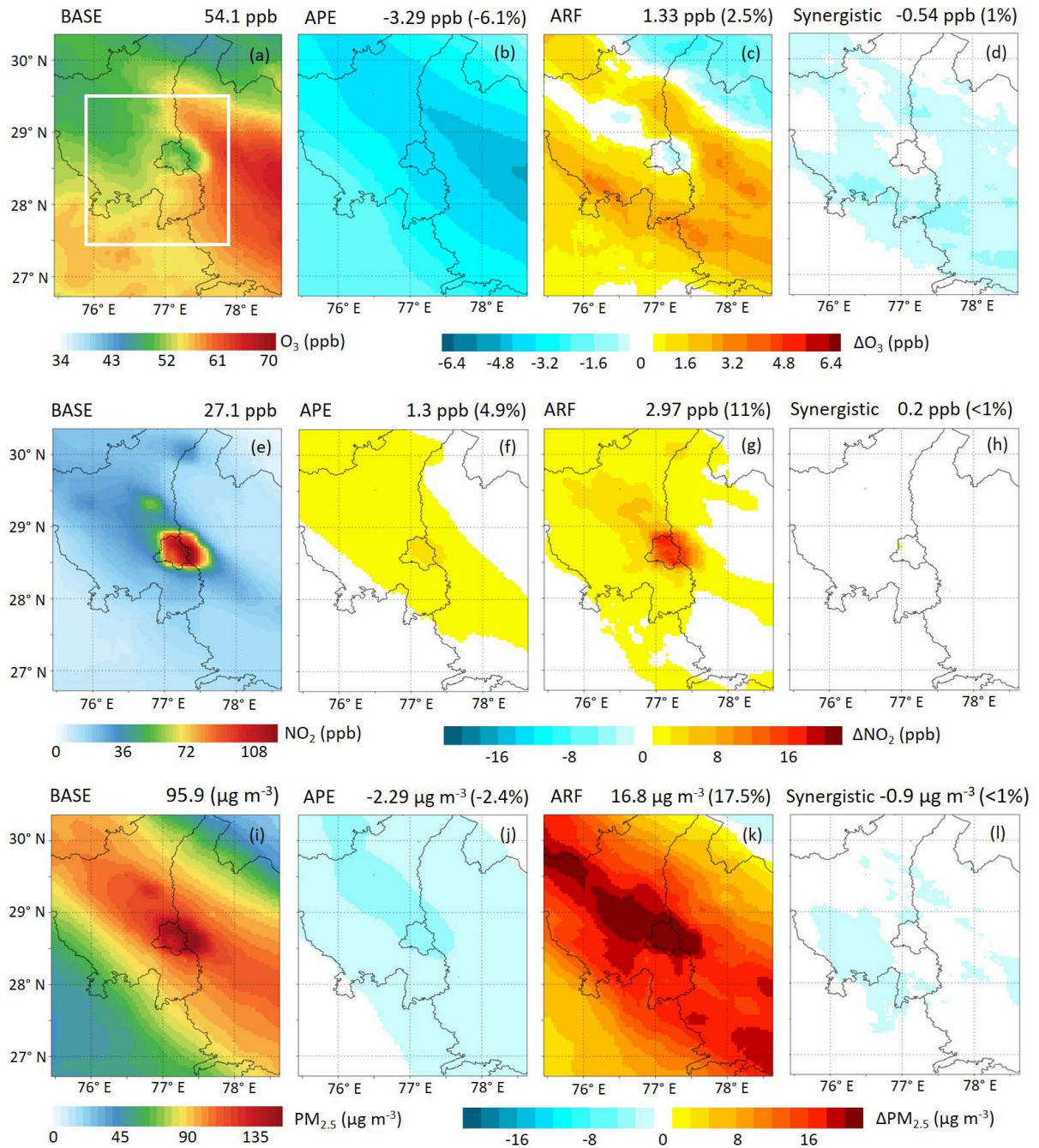
Figures 1(c–d) illustrate the monthly averaged diurnal variation of observed and simulated surface $PM_{2.5}$ and O_3 concentrations in megacity Delhi during November 2018. The UI-WRF-Chem captured the observed diurnal variations of surface O_3 and $PM_{2.5}$ with a good correlation (of 0.96 – 0.97 and 0.52 – 0.62, respectively) in both BASE and NOALL simulations (Figure 1c–d and Table S3). However, the model overestimates the daytime O_3 peak in both simulations (MB of 16 ppb in the NOALL case), with relatively less bias in the BASE case (MB of 11 ppb). Additionally, the peak of the observed $PM_{2.5}$ mass related to the morning rush hour traffic emissions is not captured well by the UI-WRF-Chem. Nevertheless, the modeled correlation of diurnal variation with observation has coefficients of 0.52 – 0.62. The differences between the model and observation could be associated with uncertainties in the input emissions, boundary layer processes, meteorology, and chemical processes. Furthermore, the absolute levels of O_3 and $PM_{2.5}$ simulated here are also consistent with the earlier model-based studies in this region (Hakim et al., 2019; Ojha et al., 2020). However, the model performed better in the BASE

179   experiment i.e., when both the APE and ARF are considered. The overall NMB between the

180   model and observed O_3 is reduced from 20% in NOALL to 13% in the BASE experiment.

181   Similarly, the NMB decreased from 12% in NOALL to 2% in the BASE simulation for $PM_{2.5}$.

182   This supports previous findings by Kumar et al. (2020) where they have reported that ARF can

183   lead to ~21–25% reduction in the mean bias of the $PM_{2.5}$ forecast in Delhi; however, the APE

184   effects on O_3 and the synergistic APE and ARF effects were not quantified in their study. The

185   contrast between BASE and NOALL suggests that UI-WRF-Chem has the fidelity needed to

186   study the role of APE and ARF toward the improvement of UI-WRF-Chem simulation of surface

187   O_3 and $PM_{2.5}$.

188   **3.2 Pure contribution of APE and ARF**

189   Figures 2(b, c, f, g, j, k) and Table 1 illustrate the pure contribution of APE and ARF on

190   surface O_3, NO_2, and $PM_{2.5}$ concentrations over NCR Delhi. The pure APE contributed to a

191   reduction in the O_3 concentration by 3.29 ppb (6.1%) via weakening the efficiency of the

192   photolytic reaction. In the pure APE scenario, the surface photolysis rates $J[NO_2]$ and $J[O^1D]$ are

193   decreased by ~23% over NCR Delhi (Figure S2a, d, Table1) which in turn reduces the surface O_3

194   and OH radical concentration (Figure S2g). The reduction in $J[NO_2]$ and $J[O^1D]$ is particularly

195   significant (Figure S3) during the early morning (07:30 – 08:30 LT) and late afternoon hours

196   (15:30 –16:30 LT, i.e., when the solar zenith angle is at around 60°), signifying the influence of

197   long path length of aerosol optical extinction for incoming UV radiation (Li et al., 2011). In

198   contrast, the pure impact of ARF increases surface O_3 over most areas of the simulated domain

199   by up to 3 ppb but slightly decreases in the megacity Delhi by up to 0.5 ppb. Overall ARF

200   increases the surface O_3 by 2.5% over the entire simulated domain (Figure 2c). This results

201   primarily from the reduction of the boundary layer height and surface energy budget by ARF

202   (Figure S4). The aerosol-induced solar dimming (–47 Wm^{-2}) leads to a cooling of –1°K at the

203   surface and decreases the surface wind speed (–0.11 ms^{-1}) and the noontime boundary layer by

204   ~143 m over the simulated domain (Figure S4). The reduced ventilation due to the shallower

205   atmospheric boundary layer and weaker winds caused by the ARF enhances the precursor levels

206   resulting in greater O_3 chemical formation. Contrarily, in megacity Delhi, which is a VOC-

207   limited regime (Nelson et al., 2021), increased NOx (see Figure 2g) concentrations at the surface

208   associated with the ARF inhibit O_3 formation due to the enhanced titration by NO. However, the

209   O$_3$ reduction due to ARF in megacity Delhi is far less significant than the changes caused by

210   APE.

Figure 2. Spatial distribution of the monthly mean concentrations of O$_2$ (upper panel), NO$_2$

(middle panel), and PM$_{2.5}$ (lower panel) averaged during the daytime (07:30–17:30 LT) in

November 2018. **(a, e, i)** are from BASE simulation; **(b, f, j)** are the change of concentrations

due to the pure APE, **(c, g, k)** are similar to (b, f, j) but due to the pure ARF, and **(d, h, l)** are the

216   changes due to the synergistic APE and ARF. The calculated values averaged over NCR Delhi

217   (denoted as white box panel (a)) are shown at the top of each panel.

Contribution	O_3 (ppb)	$PM_{2.5}$ ($\mu g\ m^{-3}$)	NO_2 (ppb)	Sulfate ($\mu g\ m^{-3}$)	Nitrate ($\mu g\ m^{-3}$)	Ammonium ($\mu g\ m^{-3}$)	$J[NO_2]$ ($10^{-3}\ s^{-1}$)	$J[O^1D]$ ($10^{-6}\ s^{-1}$)	OH (ppt)
BASE	54.11	95.9	27.14	4.258	40.175	13.29	3.898	9.519	0.075
Pure ARF	1.33	16.77	2.97	0.26	10.397	3.118	0.003	–0.084	–0.0068
Pure APE	–3.29	-2.29	1.3	-0.25	–1.60	–0.558	–0.872	–2.26	–0.024
Synergistic APE & ARF	–0.54	–0.89	0.2	-0.029	–0.64	–0.197	–0.024	–0.044	–0.0007

218   **Table 1.** Pure and synergistic contributions of APE and ARF on O_3, $PM_{2.5}$, NO_2, SNA,

219   photolysis rates, and OH radical concentration

220   In the case of $PM_{2.5}$, pure ARF contributed substantially to the $PM_{2.5}$ accumulation near

221   the surface with an average contribution of 17.5 % (16.8 $\mu g\ m^{-3}$) over the simulated domain

222   (Figure 2k). The pure impact of ARF on $PM_{2.5}$ is prominent in the megacity Delhi contributing

223   more than 20%. The increased atmospheric stability due to the pure ARF hinders the $PM_{2.5}$

224   dispersion and subsequently aggravates $PM_{2.5}$ pollution near the surface. On the other hand, pure

225   APE inhibits the $PM_{2.5}$ concentrations and leads to a decrease of 2.4% (2.29 $\mu g\ m^{-3}$). To

226   corroborate this finding, changes in the secondary inorganic aerosols such as sulfate, nitrate, and

227   ammonium (SNA) in the pure ARF and APE scenarios are analyzed (Figure S5). Bawase et al.

228   (2021) reported that SNA ions (31.44 ± 20.69 $\mu g\ m^{-3}$) are one of the largest contributors to $PM_{2.5}$

229   along with organic matter in Delhi. SNA are mostly produced in the atmosphere through

230   oxidation (including OH, and NO_3 emitted from the photolysis reactions) and neutralization of

231   precursor gases (such as SO_2, NO_2, and NH_3). As seen in Figure S5 and Table 1, pure ARF

232   substantially enhances the surface SNA concentration while pure APE leads to a slight reduction.

233   On average, sulfate, nitrate, and ammonium concentrations are increased by 0.26 $\mu g\ m^{-3}$ (6.1%),

234   10.4 $\mu g\ m^{-3}$ (25.9%), and 3.1 $\mu g\ m^{-3}$ (23%), respectively due to pure ARF. The extent of SNA

235   changes due to APE is relatively smaller than the changes caused by the pure ARF effect. Pure

236   APE decreases sulfate, nitrate, and ammonium concentration by 0.25 $\mu g\ m^{-3}$ (5.9%), 1.6 $\mu g\ m^{-3}$

237   (4%) and 0.56 μg m^{-3} (4.2%), respectively. The lower abundances of atmospheric oxidants due to

238   the modification of photolysis by pure APE decreases the rate of SNA formation and

239   subsequently alleviates the PM$_{2.5}$ concentrations near the surface.

240   **3.3 Synergistic contribution of APE and ARF**

241   The synergistic impact includes the mutual interactions between the APE and ARF.

242   Figures 2(d, h, l) illustrate the synergistic contribution of APE and ARF on surface O$_3$, NO$_2$, and

243   PM$_{2.5}$ concentrations. The synergistic APE and ARF result in an overall decrease of –0.54 ppb

244   (1%) in the monthly mean surface O$_3$ concentration averaged during the daytime (07:30–17:30

245   LT). In the case of daily peak (13:30–16:30 LT) O$_3$, the synergistic APE and ARF contributed –

246   0.8 ppb of total concentration (Figure S6d). However, in VOC-limited regimes such as in

247   megacity Delhi, the synergistic impact is nearly insignificant (<0.5%) (Figures 2d and S6d).

248   Similarly, the synergistic APE and ARF have negligible effect on modifying the photolysis rates

249   (<0.5%) (Figure S2c, f) and consequently little impact on the OH radical (1%) (Figure S2i) and

250   secondary particulate concentration (< 2%) (Figures S5 d, h, l). In the case of NO$_2$ and PM$_{2.5}$, the

251   synergistic impact contributed less than ±1 % of the total concentrations. Overall, the calculated

252   synergistic impact of APE and ARF contributed very little to the O$_3$ and PM$_{2.5}$ concentrations

253   and the impact is far less significant than pure APE and ARF impact.

254   **3.4 Discussions**

255   Figure S7 summarizes the different pathways of APE and ARF affecting O$_3$ and PM$_{2.5}$.

256   The ARF cools the surface, reduces turbulent mixing, and is conducive to the increase of relative

257   humidity (see Figure S4g), all of which are contributory to the enhancement in surface PM$_{2.5}$ and

258   precursor gas concentration. The enhanced chemical loss via strong NO titration effect (NO +O$_3$

259   →NO$_2$+O$_2$) associated with the high NOx emissions plays a critical role in weakening O$_3$

260   production in the megacity Delhi.

261   In the case of pure APE, the weakening O$_3$ and OH concentration further impedes the

262   secondary aerosol formations and subsequently alleviates the near-surface PM$_{2.5}$ concentrations.

263   A substantial reduction (~23%) in surface J[NO$_2$] due to APE has been observed in Beijing,

264   China during haze events further hindering the secondary aerosols (3.5–9.4%) and PM$_{2.5}$ (4.2%)

265   concentrations (Wu et al., 2020), which is consistent with our results. The pure contributions of

266 APE and ARF on surface O_3 as a function of $PM_{2.5}$ in megacity Delhi (See Figure S8) further

267 show that the extent of O_3 changes due to APE is larger than ARF. The APE-induced O_3

268 reduction is higher when surface $PM_{2.5}$ can reach high levels larger than 180 $\mu g\ m^{-3}$ (Figure S8).

269 Relatively strong APE effects on the surface O_3 formation compared to ARF have also been

270 reported in North China (Yang et al., 2022); however, the synergistic effects were not quantified

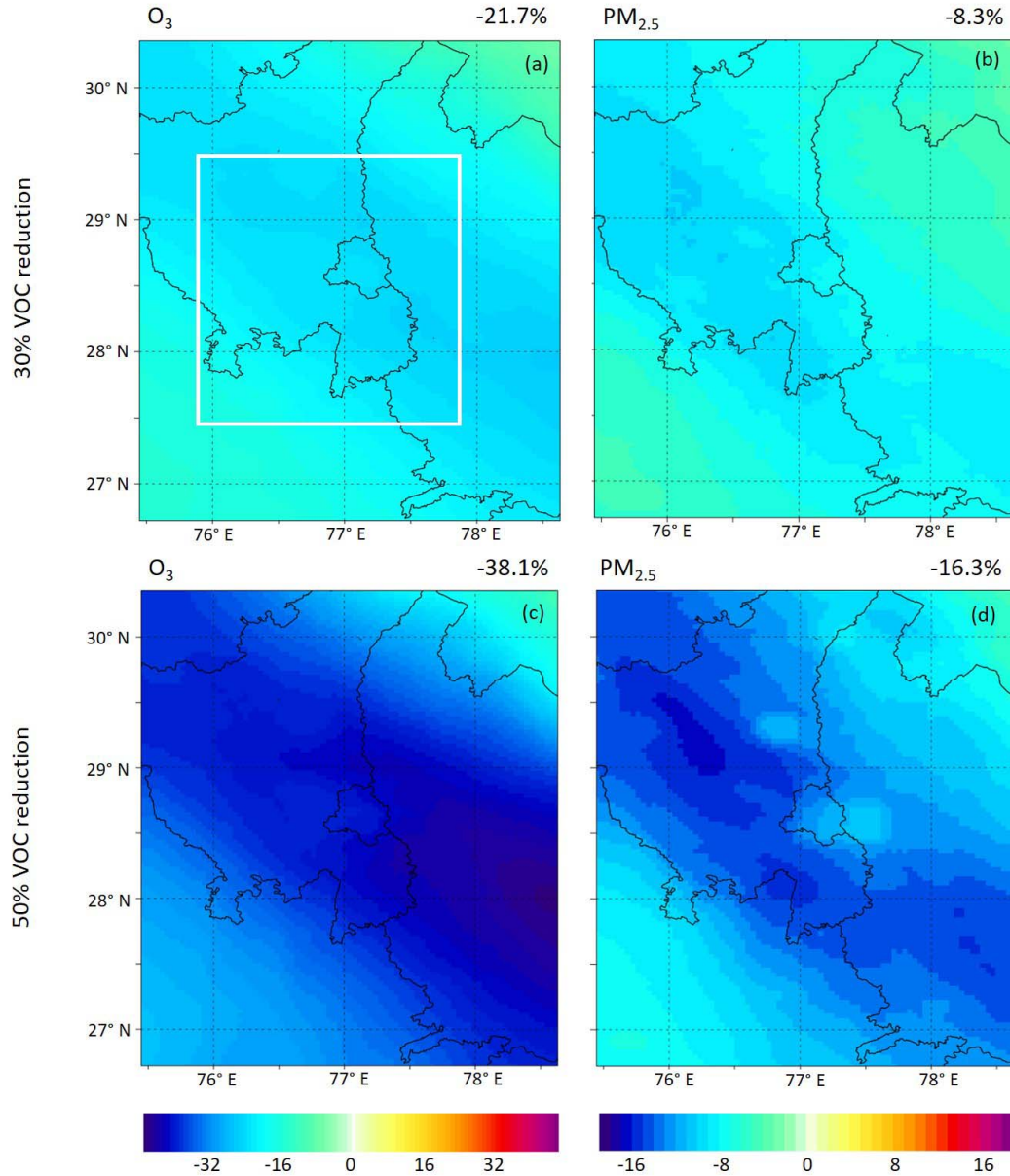271 in   their   study.

272

273 **Figure 3. (a, c)** O_3 and **(b, d)** $PM_{2.5}$ responses to the 30% and 50% reduction of VOC emissions

274 over NCR Delhi in November 2018.

275   Overall, the elucidation of the role of APE and ARF shows the importance of a

276   simultaneous mitigation strategy to co-control both O_3 and $PM_{2.5}$ concentrations in the megacity

277   Delhi. The results suggest that $PM_{2.5}$ reduction may lead to O_3 escalations due to the weakened

278   ARI. Since surface O_3 formation in Delhi is VOC limited and VOCs are common precursors for

279   both O_3 and $PM_{2.5}$, effective control of VOC emissions is required to counterbalance future O_3

280   escalations. To examine the O_3 and $PM_{2.5}$ responses to VOC emission reduction, we have

281   performed two more sensitivity experiments by reducing VOC anthropogenic emissions by 30%

282   and 50% (Figure 3 and Figure S9). The 30% VOC reduction scenario showed a decrease in

283   surface O_3 concentration by 21% over NCR Delhi. The O_3 decrease became 38% in the 50%

284   VOC emission reduction scenario and leads to a large decrease (48%) in the OH radical

285   concentration (Figure S10). As OH is the key reactive species in the formation of secondary

286   inorganic aerosols, the reduction in VOC emissions by 30–50% reduces the sulfate, nitrate, and

287   ammonium concentration by 12–26% (See Figure S11). As a result, the 30% and 50% reduction

288   of VOC leads to a decrease in $PM_{2.5}$ concentration by 8% and 16%, respectively over NCR Delhi

289   (Figure 3b, d). A recent analysis over Delhi (Chen et al., 2020) showed that a reduction in local

290   traffic emission by 50% alone reduces $PM_{2.5}$ concentration by 15–30% in Delhi but increases O_3

291   by 20–25%. However, the reduction in emissions of regional transport of pollution from the

292   NCR surrounding Delhi by 25–30% at the same time while reducing traffic emissions in Delhi

293   would further reduce $PM_{2.5}$ by 5–10% and avoid the O_3 increase (Chen et al., 2020) in line with

294   our result. Our study suggests that effective control of VOC emission helps in achieving O_3

295   reduction directly and also indirectly via weakening ARF effects from the reduced $PM_{2.5}$,

296   emphasizing the need and efficacy of VOC control for simultaneous mitigation of O_3 and $PM_{2.5}$

297   in Delhi.

298   **4   Summary and conclusions**

299   The pure and synergistic impacts of APE and ARF on surface O_3 and $PM_{2.5}$ are quantified

300   using a regional model UI-WRF-Chem employing the FSA method over NCR Delhi in

301   November 2018. The model performance in simulating surface O_3 and $PM_{2.5}$ is improved after

302   the inclusion of ARI (both APE and ARF) with a significant reduction in mean bias in the

303   megacity Delhi. The results reveal that APE reduces the surface O_3 and $PM_{2.5}$ concentrations by

304   6% and 2.4%, respectively over NCR Delhi. On the other hand, the increased atmospheric

305 stability due to ARF hinders the pollutants outflow and enhances the $PM_{2.5}$ (17.5%) and O_3

306 (2.5%) concentrations. The synergistic APE and ARF contributed very little (~1%) to the surface

307 O_3 and $PM_{2.5}$ concentration. This study implies that reducing $PM_{2.5}$ concentrations may lead to

308 O_3 escalation due to weakened aerosol radiation interactions. Considering the remarkable impact

309 of APE and ARF on O_3 and $PM_{2.5}$, these effects need to be considered in designing policies for

310 co-controlling O_3 and $PM_{2.5}$. Reducing VOC emissions (by 50%) results in a decrease in the

311 oxidant levels (38–48% decrease in O_3 and OH) and secondary aerosols (26%) and leads to a

312 16% $PM_{2.5}$ reduction, highlighting the effectiveness of VOC control in achieving O_3 and $PM_{2.5}$

313 reductions in Delhi.

314   This study provides first-hand information on evaluating the APE and ARF effects on O_3

315 and $PM_{2.5}$ using a meteorology–chemistry modeling framework in Delhi. The elucidation of the

316 role of APE and ARF is particularly significant to understand the complex $PM_{2.5}$–O_3 nexus over

317 polluted regions and the co-benefits attributed to the reduction in both pollutants. However, other

318 factors such as heterogeneous reactions associated with aerosol and aerosol-cloud interactions

319 also need to be considered for further insights into the impact of aerosol radiative effects on O_3

320 and $PM_{2.5}$ concentration.

Open Research

327 The authors acknowledge the Central Pollution Control Board (CPCB) of India

328 (https://app.cpcbccr.com/ccr/#/caaqm-dashboard-all/caaqm-landing) for $PM_{2.5}$, O_3, T2, and RH

329 data. WRF-Chem is an open-access model which can be acquired at

330 https://www2.acom.ucar.edu/wrf-chem. The authors thank NASA for making MERRA-2

331 reanalysis (https://gmao.gsfc.nasa.gov/reanalysis/MERRA-2/) and GLDAS

332 (https://disc.gsfc.nasa.gov/datasets?keywords=GLDAS) data publicly accessible. The EDGAR-

333 HTAP v2 anthropogenic emissions were obtained from
334 https://edgar.jrc.ec.europa.eu/dataset_htap_v2.

335 **References**

336 Bawase, M., Sathe, Y., Khandaskar, H., & Sukrut, T. (2021). Chemical composition and source
337   attribution of PM$_{2.5}$ and PM$_{10}$ in Delhi-National Capital Region (NCR) of India: results
338   from an extensive seasonal campaign. *J Atmos Chem, 78*, 35–58.
339   https://doi.org/10.1007/s10874-020-09412-7

340 Benas, N., Mourtzanou, E., Kouvarakis, G., Bais, A., Mihalopoulos, N., & Vardavas, I. (2013).
341   Surface ozone photolysis rate trends in the Eastern Mediterranean: Modeling the effects
342   of aerosols and total column ozone based on Terra MODIS data. *Atmospheric
343   Environment, 74*, 1-9. doi:https://doi.org/10.1016/j.atmosenv.2013.03.019

344 Bharali, C., Nair, V. S., Chutia, L., & Babu, S. (2019). Modeling of the Effects of Wintertime
345   Aerosols on Boundary Layer Properties Over the Indo Gangetic Plain. *Journal of
346   Geophysical Research: Atmospheres, 124*. doi:10.1029/2018JD029758

347 Bran, S. H., & Srivastava, R. (2017). Investigation of PM(2.5) mass concentration over India
348   using a regional climate model. *Environ Pollut, 224*, 484-493.
349   doi:10.1016/j.envpol.2017.02.030

350 Chen, Y., Wild, O., Ryan, E., Sahu, S. K., Lowe, D., Archer-Nicholls, S., . . . Beig, G. (2020).
351   Mitigation of PM2.5 and ozone pollution in Delhi: a sensitivity study during the pre-
352   monsoon period. *Atmos. Chem. Phys., 20*(1), 499-514. doi:10.5194/acp-20-499-2020

353 Chou, M.-D., & Suarez, M. J. (1994). An efficient thermal infrared radiation parameterization
354   for use in general circulation models. *NASA Technical Memorandum 104606, 3,* 85.
355   https://archive.org/details/nasa_techdoc_19950009331

356 Chutia, L., Ojha, N., Girach, I. A., Sahu, L. K., Alvarado, L. M. A., Burrows, J. P., . . . Bhuyan,
357   P. K. (2019). Distribution of volatile organic compounds over Indian subcontinent during
358   winter: WRF-chem simulation versus observations. *Environ Pollut, 252*(Pt A), 256-269.
359   doi:10.1016/j.envpol.2019.05.097

360 Conibear, L., Butt, E. W., Knote, C., Arnold, S. R., & Spracklen, D. V. (2018). Residential
361   energy use emissions dominate health impacts from exposure to ambient particulate
362   matter in India. *Nature Communications, 9*(1), 617. doi:10.1038/s41467-018-02986-7

363   Dickerson, R. R., Kondragunta, S., Stenchikov, G., Civerolo, K. L., Doddridge, B. G., & Holben,
364   B. N. (1997). The impact of aerosols on solar ultraviolet radiation and photochemical
365   smog. *Science, 278*(5339), 827-830. doi:10.1126/science.278.5339.827

366   Flynn, J., Lefer, B., Rappenglück, B., Leuchner, M., Perna, R., Dibb, J., . . . Crawford, J. (2010).
367   Impact of clouds and aerosols on ozone production in Southeast Texas. *Atmospheric
368   Environment, 44*(33), 4126-4133. doi:https://doi.org/10.1016/j.atmosenv.2009.09.005

369   Ge, C., Wang, J., & Reid, J. (2013). Mesoscale modeling of smoke transport over the Southeast
370   Asian Maritime Continent: Coupling of smoke direct radiative feedbacks below and
371   above the low-level clouds. *Atmospheric Chemistry & Physics Discussions, 13*, 15443-
372   15492. doi:10.5194/acpd-13-15443-2013

373   Ge, C., Wang, J., Reid, J. S., Posselt, D. J., Xian, P., & Hyer, E. J. (2017). Mesoscale modeling
374   of smoke transport from equatorial Southeast Asian Maritime Continent to the
375   Philippines: First comparison of ensemble analysis with in situ observations. *Journal of
376   Geophysical Research, 122*, 5380-5398.

377   Ghude, S. D., Chate, D. M., Jena, C., Beig, G., Kumar, R., Barth, M. C., . . . Pithani, P. (2016).
378   Premature mortality in India due to PM2.5 and ozone exposure. *Geophysical Research
379   Letters, 43*(9), 4650-4658. doi:https://doi.org/10.1002/2016GL068949

380   Hakim, Z. Q., Archer-Nicholls, S., Beig, G., Folberth, G. A., Sudo, K., Abraham, N. L., . . .
381   Archibald, A. T. (2019). Evaluation of tropospheric ozone and ozone precursors in
382   simulations from the HTAPII and CCMI model intercomparisons – a focus on the Indian
383   subcontinent. *Atmos. Chem. Phys., 19*(9), 6437-6458. doi:10.5194/acp-19-6437-2019

384   Janssens-Maenhout, G., Crippa, M., Guizzardi, D., Dentener, F., Muntean, M., Pouliot, G., . . .
385   Li, M. (2015). HTAP_v2.2: a mosaic of regional and global emission grid maps for 2008
386   and 2010 to study hemispheric transport of air pollution. *Atmos. Chem. Phys., 15*(19),
387   11411-11432. doi:10.5194/acp-15-11411-2015

388   Jat, R., Gurjar, B. R., & Lowe, D. (2021). Regional pollution loading in winter months over India
389   using high resolution WRF-Chem simulation. *Atmospheric Research, 249*, 105326.
390   doi:https://doi.org/10.1016/j.atmosres.2020.105326

391   Krishna, R. K., Ghude, S. D., Kumar, R., Beig, G., Kulkarni, R., Nivdange, S., & Chate, D.
392   (2019). Surface PM2.5 Estimate Using Satellite-Derived Aerosol Optical Depth over
393   India. *Aerosol and Air Quality Research, 19*(1), 25-37. doi:10.4209/aaqr.2017.12.0568

Kulkarni, S. H., Ghude, S. D., Jena, C., Karumuri, R. K., Sinha, B., Sinha, V., . . . Khare, M. (2020). How Much Does Large-Scale Crop Residue Burning Affect the Air Quality in Delhi? *Environ Sci Technol, 54*(8), 4790-4799. doi:10.1021/acs.est.0c00329

Kumar, R., Ghude, S. D., Biswas, M., Jena, C., Alessandrini, S., Debnath, S., . . . Rajeevan, M. (2020). Enhancing Accuracy of Air Quality and Temperature Forecasts During Paddy Crop Residue Burning Season in Delhi Via Chemical Data Assimilation. *Journal of Geophysical Research: Atmospheres, 125*(17), e2020JD033019. doi:https://doi.org/10.1029/2020JD033019

Li, G., Bei, N., Tie, X., & Molina, L. T. (2011). Aerosol effects on the photochemistry in Mexico City during MCMA-2006/MILAGRO campaign. *Atmos. Chem. Phys., 11*(11), 5169-5182. doi:10.5194/acp-11-5169-2011

Li, G., Zhang, R., Fan, J., & Tie, X. (2005). Impacts of black carbon aerosol on photolysis and ozone. *Journal of Geophysical Research: Atmospheres, 110*(D23).

Li, N., He, Q., Greenberg, J., Guenther, A., Li, J., Cao, J., . . . Zhang, Q. (2018). Impacts of biogenic and anthropogenic emissions on summertime ozone formation in the Guanzhong Basin, China. *Atmos. Chem. Phys., 18*(10), 7489-7507. doi:10.5194/acp-18-7489-2018

Li, Z., Guo, J., Ding, A., Liao, H., Liu, J., Sun, Y., . . . Zhu, B. (2017). Aerosol and boundary-layer interactions and impact on air quality. *National Science Review, 4*(6), 810-833. doi:10.1093/nsr/nwx117

Liao, H., Yung, Y., & Seinfeld, J. (1999). Effect of Aerosols on Tropospheric Photolysis Rates in Clear and Cloudy Atmospheres. *Journal of Geophysical Research, 1042*, 23697-23708. doi:10.1029/1999JD900409

Liu, Q., Jia, X., Quan, J., Li, J., Li, X., Wu, Y., . . . Liu, Y. (2018). New positive feedback mechanism between boundary layer meteorology and secondary aerosol formation during severe haze events. *Scientific Reports, 8*(1), 6095. doi:10.1038/s41598-018-24366-3

Mogno, C., Palmer, P. I., Knote, C., Yao, F., & Wallington, T. J. (2021). Seasonal distribution and drivers of surface fine particulate matter and organic aerosol over the Indo-Gangetic Plain. *Atmos. Chem. Phys., 21*(14), 10881-10909. doi:10.5194/acp-21-10881-2021

Mukherjee, T., Vinoj, V., Midya, S. K., Puppala, S. P., & Adhikary, B. (2020). Numerical simulations of different sectoral contributions to post monsoon pollution over Delhi. *Heliyon, 6*(3), e03548. doi:https://doi.org/10.1016/j.heliyon.2020.e03548

425 Nelson, B. S., Stewart, G. J., Drysdale, W. S., Newland, M. J., Vaughan, A. R., Dunmore, R. E.,
426   . . . Lee, J. D. (2021). In situ ozone production is highly sensitive to volatile organic
427   compounds in Delhi, India. *Atmos. Chem. Phys., 21*(17), 13609-13630. doi:10.5194/acp-
428   21-13609-2021

429 Ojha, N., Sharma, A., Kumar, M., Girach, I., Ansari, T. U., Sharma, S. K., . . . Gunthe, S. S.
430   (2020). On the widespread enhancement in fine particulate matter across the Indo-
431   Gangetic Plain towards winter. *Sci Rep, 10*(1), 5862. doi:10.1038/s41598-020-62710-8

432 Qu, Y., An, J., & Li, J. (2013). Synergistic impacts of anthropogenic and biogenic emissions on
433   summer surface O3 in East Asia. *Journal of Environmental Sciences, 25*(3), 520-530.
434   doi:https://doi.org/10.1016/S1001-0742(12)60069-2

435 Real, E., & Sartelet, K. (2011). Modeling of photolysis rates over Europe: impact on chemical
436   gaseous species and aerosols. *Atmos. Chem. Phys., 11*(4), 1711-1727. doi:10.5194/acp-
437   11-1711-2011

438 Reid, J. S., Hyer, E. J., Prins, E. M., Westphal, D. L., Zhang, J., Wang, J., . . . Hoffman, J. P.
439   (2009). Global Monitoring and Forecasting of Biomass-Burning Smoke: Description of
440   and Lessons From the Fire Locating and Modeling of Burning Emissions (FLAMBE)
441   Program. *IEEE Journal of Selected Topics in Applied Earth Observations and Remote
442   Sensing, 2*(3), 144-162. doi:10.1109/JSTARS.2009.2027443

443 Sahu, S. K., & Kota, S. H. (2017). Significance of PM2.5 Air Quality at the Indian Capital.
444   *Aerosol and Air Quality Research, 17*(2), 588-597. doi:10.4209/aaqr.2016.06.0262

445 Schell, B., Ackermann, I. J., Hass, H., Binkowski, F. S., & Ebel, A. (2001). Modeling the
446   formation of secondary organic aerosol within a comprehensive air quality model system.
447   *Journal of Geophysical Research: Atmospheres, 106*(D22), 28275-28293.

448 Sha, T., Ma, X., Zhang, H., Janechek, N., Wang, Y., Wang, Y., . . . Wang, J. (2021). Impacts of
449   Soil NOx Emission on O3 Air Quality in Rural California. *Environmental Science &
450   Technology, 55*(10), 7113-7122. doi:10.1021/acs.est.0c06834

451 Sharma, A., Ojha, N., Pozzer, A., Mar, K. A., Beig, G., Lelieveld, J., & Gunthe, S. S. (2017).
452   WRF-Chem simulated surface ozone over south Asia during the pre-monsoon: effects of
453   emission inventories and chemical mechanisms. *Atmos. Chem. Phys., 17*(23), 14393-
454   14413. doi:10.5194/acp-17-14393-2017

455   Sinha, B., Singh Sangwan, K., Maurya, Y., Kumar, V., Sarkar, C., Chandra, B. P., & Sinha, V.
456   (2015). Assessment of crop yield losses in Punjab and Haryana using 2 years of
457   continuous in situ ozone measurements. *Atmos. Chem. Phys., 15*(16), 9555-9576.
458   doi:10.5194/acp-15-9555-2015

459   Stein, U., & Alpert, P. (1993). Factor Separation in Numerical Simulations. *Journal of*
460   *Atmospheric Sciences, 50*(14), 2107-2115. doi:10.1175/1520-
461   0469(1993)050<2107:Fsins>2.0.Co;2

462   Stockwell, W. R., Middleton, P., Chang, J. S., & Tang, X. (1990). The second generation
463   regional acid deposition model chemical mechanism for regional air quality modeling.
464   *Journal of Geophysical Research: Atmospheres, 95*(D10), 16343-16367.

465   Tie, X., Madronich, S., Walters, S., Zhang, R., Rasch, P., & Collins, W. (2003). Effect of clouds
466   on photolysis and oxidants in the troposphere. *Journal of Geophysical Research:*
467   *Atmospheres, 108*(D20). doi:https://doi.org/10.1029/2003JD003659

468   Upadhyay, A., Dey, S., Chowdhury, S., & Goyal, P. (2018). Expected health benefits from
469   mitigation of emissions from major anthropogenic PM2.5 sources in India: Statistics at
470   state level. *Environmental Pollution, 242*, 1817-1826.
471   doi:https://doi.org/10.1016/j.envpol.2018.07.085

472   Wang, J., Ge, C., Yang, Z., Hyer, E. J., Reid, J. S., Chew, B.-N., . . . Zhang, M. (2013).
473   Mesoscale modeling of smoke transport over the Southeast Asian Maritime Continent:
474   Interplay of sea breeze, trade wind, typhoon, and topography. *Atmospheric Research,*
475   *122*, 486-503. doi:10.1016/j.atmosres.2012.05.009

476   Wang, Y., Yu, M., Wang, Y., Tang, G., Song, T., Zhou, P., . . . Petäjä, T. (2020). Rapid
477   formation of intense haze episodes via aerosol–boundary layer feedback in Beijing.
478   *Atmos. Chem. Phys., 20*(1), 45-53. doi:10.5194/acp-20-45-2020

479   Wu, J., Bei, N., Hu, B., Liu, S., Wang, Y., Shen, Z., . . . Li, G. (2020). Aerosol-photolysis
480   interaction reduces particulate matter during wintertime haze events. *Proc Natl Acad Sci*
481   *U S A, 117*(18), 9755-9761. doi:10.1073/pnas.1916775117

482   Xing, J., Wang, J., Mathur, R., Wang, S., Sarwar, G., Pleim, J., . . . Hao, J. (2017). Impacts of
483   aerosol direct effects on tropospheric ozone through changes in atmospheric dynamics
484   and photolysis rates. *Atmos. Chem. Phys., 17*(16), 9869-9883. doi:10.5194/acp-17-9869-
485   2017

486   Yang, H., Chen, L., Liao, H., Zhu, J., Wang, W., & Li, X. (2022). Impacts of aerosol–photolysis
487   interaction and aerosol–radiation feedback on surface-layer ozone in North China during
488   multi-pollutant air pollution episodes. *Atmos. Chem. Phys., 22*(6), 4101-4116.
489   doi:10.5194/acp-22-4101-2022
490   Yang, Y., Chen, M., Zhao, X., Chen, D., Fan, S., Guo, J., & Ali, S. (2020). Impacts of aerosol–
491   radiation interaction on meteorological forecasts over northern China by offline coupling
492   of the WRF-Chem-simulated aerosol optical depth into WRF: a case study during a
493   heavy pollution event. *Atmos. Chem. Phys., 20*(21), 12527-12547. doi:10.5194/acp-20-
494   12527-2020
495   Zhang, H., Wang, J., García, L. C., Zhou, M., Ge, C., Plessel, T., . . . Spero, T. L. (2022).
496   Improving Surface PM2.5 Forecasts in the United States Using an Ensemble of Chemical
497   Transport Model Outputs: 2. Bias Correction With Satellite Data for Rural Areas. *Journal*
498   *of Geophysical Research: Atmospheres, 127*(1), e2021JD035563.
499   doi:https://doi.org/10.1029/2021JD035563
500   Zhao, D., Xin, J., Gong, C., Quan, J., Liu, G., Zhao, W., . . . Song, T. (2019). The formation
501   mechanism of air pollution episodes in Beijing city: Insights into the measured feedback
502   between aerosol radiative forcing and the atmospheric boundary layer stability. *Science of*
503   *The Total Environment, 692*, 371-381. doi:https://doi.org/10.1016/j.scitotenv.2019.07.255